Applied Catalysis A, General 565 (2018) 59–67

Contents lists available at ScienceDirect

Applied Catalysis A, General

journal homepage: www.elsevier.com/locate/apcata

Controlled manipulation of enzyme specificity through immobilization-induced flexibility constraints

Cristina Coscolín[a], Ana Beloqui[b], Mónica Martínez-Martínez[a], Rafael Bargiela[a,c], Gerard Santiago[d], Rosa M. Blanco[a], Guillaume Delaittre[e,f], Carlos Márquez-Álvarez[a,*], Manuel Ferrer[a,*]

[a] Institute of Catalysis, Consejo Superior de Investigaciones Científicas, 28049 Madrid, Spain
[b] CICnanoGUNE, 20018 San Sebastián, Spain
[c] School of Chemistry, Bangor University, LL57 2UW Bangor, UK
[d] Barcelona Supercomputing Center (BSC), 08034 Barcelona, Spain
[e] Karlsruhe Institute of Technology, Institute of Toxicology and Genetics, 76344 Eggenstein-Leopoldshafen, Germany
[f] Karlsruhe Institute of Technology, Institute for Chemical Technology and Polymer Chemistry, 76131 Karlsruhe, Germany

ARTICLE INFO

Keywords:
Biocatalyst
Esterase
Immobilization
Mesoporous
Microparticles
Specificity

ABSTRACT

It is thought that during immobilization enzymes, as dynamic biomolecules, may become distorted and this may alter their catalytic properties. However, the effects of different immobilization strategies on enzyme rigidity or flexibility and their consequences in specificity and stereochemistry at large scale has not been yet clearly evaluated and understood. This was here investigated by using as model an ester hydrolase, isolated from a bacterium inhabiting a karstic lake, with broad substrate spectrum (72 esters being converted; 61.5 U mg^{-1} for glyceryl tripropionate) but initially non-enantiospecific. We found that the enzyme (7 nm × 4.4 nm × 4.2 nm) could be efficiently ionic exchanged inside the pores (9.3 nm under dry conditions) of amino-functionalized ordered mesoporous material (NH_2-SBA-15), achieving a protein load of 48 mg g^{-1}, and a specific activity of 4.5 ± 0.1 U mg^{-1}. When the enzyme was site-directed immobilized through His interaction with an immobilized cationon the surface of two types of magnetic micro-particles through hexahistidine-tags, protein loads up to 10.2 μg g^{-1} and specific activities of up to 29.9 ± 0.3 U mg^{-1}, were obtained. We found that ionically exchanged enzyme inside pores of NH_2-SBA-15 drastically narrowed the substrate range (17 esters), to an extent much higher than ionically exchanged enzyme on the surface of magnetic micro-particles (up to 61 esters). This is attributed to differences in surface chemistry, particle size, and substrate accessibility to the active site tunnel. Our results also suggested, for the first time, that immobilization of enzymes in pores of similar size may alter the enzyme structures and produce enzyme active centers with different configuration which promote stereochemical conversions in a manner different to those arising from surface immobilization, where the strength of the ionic exchange also has an influence. This was shown by demonstrating that when the enzyme was introduced inside pores with a diameter (under dry conditions) slightly higher than that of the enzyme crystal structure a biocatalyst enantiospecific for ethyl (*R*)-4-chloro-3-hydroxybutyrate was produced, a feature not found when using wider pores. By contrast, immobilization on the surface of ferromagnetic microparticles produced selective biocatalysts for methyl (*S*)-(+)-mandelate or methyl (*S*)-lactate depending on the functionalization. This study illustrates the benefits of extensive analysis of the substrate spectra to better understand the effects of different immobilization strategies on enzyme flexibility/rigidity, as well as substrate specificity and stereochemistry. Our results will help to design tunable materials and interfaces for a controlled manipulation of specificity and to transform non-enantiospecific enzymes into stereo-chemically substrate promiscuous biocatalysts capable of converting multiple chiral molecules.

* Corresponding authors.
E-mail addresses: c.marquez@icp.csic.es (C. Márquez-Álvarez), mferrer@icp.csic.es (M. Ferrer).

https://doi.org/10.1016/j.apcata.2018.08.003
Received 8 June 2018; Received in revised form 2 August 2018; Accepted 4 August 2018
Available online 06 August 2018

1. Introduction

Enzymes are delicate organic catalysts that need to be stabilized to survive a range of challenging conditions typically used in industrial processes. Multiple immobilization methods and materials have been successfully employed to generate stabilized biocatalysts [1–4], but the most efficient immobilization protocol and materials may be selected aiming at a balance between activity, specificity, stability, and costs [5]. Besides most used carriers such as (epoxy)acrylic resins and agarose and widely used nanoparticles such as chitosan and nanoflowers [6], outstanding recent examples for enzyme immobilization and stabilization included biomimetic silica supports [7], mesostructured onion-like silica [8], hybrid macroporous foams synthesized via an integrative chemistry synthetic pathway [9], superparamagnetic silica/iron oxide nanocomposites with mesostructured porosity [10], maghemite (γ-Fe_2O_3) nanoparticles functionalized with a reactive multifunctional polymer [11], dendronized polymer and mesoporous silica nanoparticles [12], carbon nanotubes and polymers [13], epoxy-activated carriers [14], borosilicate [15], hematite nanoparticles [16], phyto-inspired silica nanowires [17], and materials with bioinspired coatings [18], to cite some. These studies exemplify the large interest in designing new and more efficient carriers for enzyme immobilization, the comparative analysis of which at large, in relation to their effect in enzyme substrate specificity (including enantiospecificity), may deserve further interest.

A major advance in the last decade has been the development of enzyme encapsulation in ordered mesoporous materials, because of their high specific surface area and pore volume, their highly uniform and tunable pore sizes, and the possibility to create micropores interconnecting mesopores and to control their morphology; they are also thermally, mechanically and chemically stable [5,19–23]. Various proteins have been successfully immobilized on mesoporous materials, including, non-catalytic proteins, oxidoreductases, hydrolases, lyases and isomerases [5,24–41]. Enzymes immobilized in confined macromolecular environments where the surface and volume of the confined environment can be controlled, are suggested to constitute optimal enzymatic nanoreactors [19,42,43]. Their surface can be grafted with different functionalities [23,17,18], a property particularly interesting to allow, for example, the ionic exchange enzyme encapsulation in amino-functionalized ordered mesoporous materials. This development led to an increased enzyme loading (up to 187 mg g^{-1} of catalyst) by simply adjusting synthetic conditions of the siliceous material for the obtaining of pores large enough to permit enzyme entrance and diffusion through the pore channels [17,18]. As example, mesoporous materials with pore diameters as low as 3–10 nm and also tailored between 3–30 nm have been synthesized [for examples see ref. 19,23,25,28,29,31], and enzymes with sizes such as 6.1 nm × 5.0 nm × 4.9 nm [20] have been immobilized in the pores. In these ordered structures the enzyme is immobilized by electrostatic interactions with limited diffusional restrictions and low enzyme modification, typically occurring after covalent binding or crosslinking [44]. This ion exchange of the enzyme on the support, was demonstrated to minimize leaching and maximize activity and stability of the biocatalyst [17,18].

Compared to free enzyme in solution, immobilization on a surface often hinders the free movement of the enzyme, although it is believed that the enzyme is positioned in an environment where the inherent flexibility is high [45]. The confinement in the pores of mesoporous materials is also thought to hinder the free movement of enzyme, but to what extent the differences in movement and flexibility affects enzyme properties remains to be elucidated. In this direction, it is only supposed that larger substrates may be preferably hydrolyzed by enzymes immobilized on the external surface or at the entrance of the channels of mesoporous materials because of substrate diffusional and enzyme orientation issues, as it was demonstrated by modelling predictions [46] and also using a lipase when tested with small (tributyrin) and large (triolein) substrates [47]. However, a general overview about how enzyme immobilization inside pores affects substrate specificity compared to the free enzyme and surface-immobilized enzyme remains to be established. Indeed, diverse surface immobilization methods have been shown to preserve activity level and, most importantly, to even create enantiospecific enzymes such as lipases [for example see ref. 48–50]. These, and other studies, have been performed using a restricted set of molecules and a comparative analysis at large is lacking.

Here, we examine the substrate range and enantiospecificity of a target enzyme by using as supports, an amino-functionalized ordered mesoporous material (NH_2-SBA-15) allowing non-covalent enzyme immobilization inside pores and two types of magnetic microparticles for non-covalent surface immobilization. Particularly, agarose-coated ferromagnetic core-shell microparticles with a nitrilotetracetic acid (NTA) tetradentate ligand, and polyvinyl alcohol microparticles embedded with magnetite and grafted with an iminodiacetic acid (IDA) tridentate ligand. Both particles were Ni^{2+}-activated and thus can be used for purification and immobilization given the affinity for hexahistidine-tags. As model enzyme, a serine ester hydrolase isolated from the metagenomic DNA of microbial communities inhabiting a karstic lake [51], referred to as EH1, with a typical α/β hydrolase fold as a model. Its structure was recently solved (PDB code 5JD4) [51,52], and in a recent study it was identified as one of the ester hydrolases with broader substrate spectrum among a total of 147 when tested with a set of 96 chemically and structurally different esters [51]. The active site (catalytic triad: Ser161, Asp256 and His286; oxyanion hole: Gly88, Gly89 and Gly90) supports the hydrolysis of a broad range of 72 esters, with vinyl butyrate (200.7 ± 0.4 U mg^{-1}) and phenyl propionate (198.7 ± 0.9 U mg^{-1}) serving as the best substrates (Table S1). Being highly promiscuous in terms of substrate scope, EH1 is not enantiospecific; thus the apparent enantiospecificity (E_{app}) factor calculated as the ratio of specific activities for 14 chiral esters when pure stereoisomers were tested separately [53] was below 25, a value above which ester hydrolases begin to have practical value [54]. Based on these considerations, EH1 may be then considered as an ester hydrolase with prominent substrate promiscuity but with limited practical use due to the low stereospecificity. Because substrate promiscuity and enantiospecificity are two appreciated properties when combined in a single biocatalyst, which is rare in nature within esterases [54], we evaluated whether both properties can be tailored by employing three immobilization strategies.

To the best of our knowledge, detailed analysis of the substrate spectrum and interpretation of the data provides, for the first time, new insights into the contribution of chemical, physical, and flexibility constrains to the catalytic capacity of biocatalysts prepared by these immobilization methods. We would like to highlight that the effect of immobilization on enzyme flexibility has been previously studied, for example, by increasing the number of bonds by which the enzyme is linked to the surface of carriers [48–50]. It is though that this increases enzyme rigidity and in turn has a consequence in promoting enzyme stability and activity when tested over a specific set of substrates [48–50]. The novelty of this study is that through an analysis of the substrate specificity with a very broad spectrum of molecules, and 3 different immobilization techniques, we were able to demonstrate that each polymeric carrier induced different flexibility and rigidity constraints to the enzyme with distinct effects on specificity and, most importantly, enantiospecificity, which can be also controlled.

2. Experimental section

2.1. Chemicals and EH1 protein source

All chemicals used for enzymatic tests were of the purest grade available and were purchased from sources described elsewhere [51]. The isolation of the enzyme EH1, available in the expression plasmid pET46 Ek/LIC and *Escherichia coli* BL21 as a host, was reported previously [51,52].

2.2. Gene expression and protein purification

Expression of the gene encoding the N-terminally hexahistidine-tagged enzyme and purification were performed as previously described [51,52]. Purity was assessed as > 98% using SDS-PAGE analysis in a Mini PROTEAN electrophoresis system (Bio-Rad) [55]. The protein concentration was determined according to Bradford assay with bovine serum albumin as a standard [56].

2.3. Synthesis and characterization of the mesostructured silica support and EH1 immobilization

Mesoporous silica with a periodic arrangement of uniform-diameter pore channels (SBA-15 mesostructure) was synthesized according to the method reported by Linton and Alfredsson [57]. A 2.5 wt% aqueous solution of Pluronic PE-10400 (BASF) surfactant was prepared by carefully dissolving this compound in a 1.6 M HCl solution, at 35 °C, in a closed polypropylene container kept under magnetic stirring for 2 h. Tetramethyl orthosilicate (TMOS, 98%, Aldrich) was added to this solution (3.8 g TMOS in 100 g of surfactant solution) and the mixture kept at 55 °C for 20 h under magnetic stirring. The white solid product formed was aged in the mother liquor at 75 °C for 24 h without stirring. Finally, the solid was filtered off, washed with absolute ethanol (Panreac) and calcined in air in a muffle furnace at 550 °C for 6 h using a 2 °C min^{-1} heating ramp. The white powder obtained is labelled "SBA-15".

Powder X-ray diffraction (XRD) pattern of SBA-15 silica (Fig. 1) were recorded at low angle (0.4-6°, step size 0.0167°) with a PANalytical X'Pert Pro diffractometer using CuKα radiation with a nickel filter. The pattern confirms that the pore channels arrangement exhibits p6mm hexagonal symmetry. It shows an intense peak at a 2θ angle of 0.9° corresponding to the d_{100} spacing and two weak reflections at 2θ close to 1.5° and 1.7°, assigned to the d_{110} and d_{200} spacing, respectively. From these data, the calculated unit-cell lattice parameter a_0 is 11.3 nm. Note that the unit-cell lattice parameter a_0 corresponds to the distance between the centers of two neighboring cylindrical pore channels (that is, the sum of the pore diameter and of the width of the silica pore wall that separates two channels).

Scanning electron microscopy (SEM) images were recorded using a FEI Nova NanoSEM 230 FE-SEM microscope equipped with vCD detector. These images show (Fig. 2, left) the plate-like shape of silica particles. Platelets were several microns wide and their thickness was close to 200 nm. Transmission electron microscopy (TEM) images (obtained with a JEOL JEM-2100 electron microscope operated at 200 kV) showed (Fig. 2, right) that the mesopore channels exhibit a long-range 2D hexagonal arrangement, in agreement with XRD data, and that these channels run parallel to the short axis of the platelets.

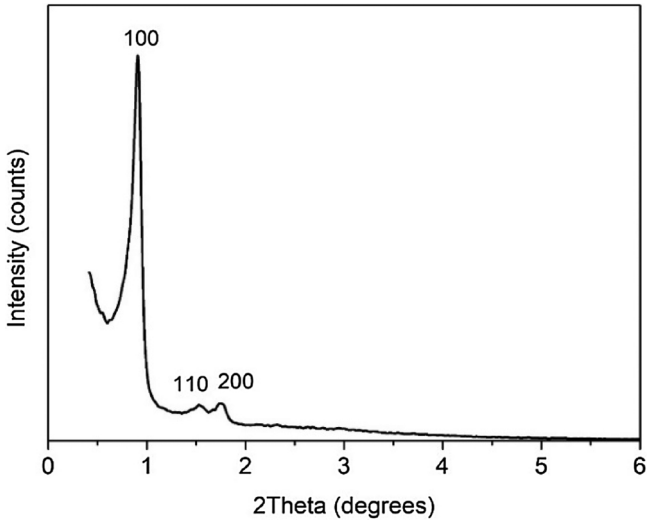

Fig. 1. XRD pattern of SBA-15 silica.

Nitrogen adsorption-desorption isotherm of SBA-15 silica (Fig. 3) was acquired at 77 K with a Micromeritics ASAP 2420 sorptometer. Prior to analysis, the sample was degassed at 623 K for 16 h. The isotherm obtained is of the type IVa according to 2015 IUPAC classification [58]. This type of isotherm shows a steep increase of the adsorbed volume (that takes place at a relative pressure around 0.7 in the isotherm plotted in Fig. 3), due to capillary condensation in mesopores, together with a hysteresis loop that is consistent with the presence of cylindrical mesopores. Pore size distribution (Fig. 3, inset) was obtained from the adsorption data using the methods of non-local density functional theory (NLDFT) with the kernel function for oxide materials with cylindrical pores [59,60]. The narrow distribution obtained indicates that the dried mesoporous silica possesses pore channels with a highly uniform diameter close to 9.3 nm. DFT calculations also indicated that mesopores account for a total volume of 0.44 $cm^3 g^{-1}$ and that the sample exhibits some micro-porosity (as expected for SBA-15 silica) accounting for an additional volume of 0.1 $cm^3 g^{-1}$.

The SBA-15 silica sample was functionalized with aminopropyl groups by grafting with an alkoxysilane. The silica powder (0.833 g) was placed inside a round bottom flask and dried overnight under vacuum (ca. 10^{-2} mbar) at 80 °C. Then, 50 mL of toluene (anhydrous, 99.8%, Sigma-Aldrich) were added to the flask and the solid kept in suspension with magnetic stirring under dry nitrogen atmosphere. To this suspension, 1.0 mL of 3-aminopropyl)triethoxysilane (APTES, 99%, Aldrich) was added (equivalent to 5 mmol alkoxysilane per gram of silica) and the mixture kept under reflux for 24 h. The solid was finally filtered off and washed with dry toluene and acetone. The content of amino groups in the functionalized sample was determined to be 1.0 mmol g^{-1}, as measured by CHN elemental analysis using a LECO CHNS-932 equipment. This sample, labelled "NH_2-SBA-15", was used as support for immobilization of EH1.

Briefly, a total of 0.96 mL of esterase solution (5 mg mL^{-1}) was added to 10.04 mL of 40 mM HEPES buffer pH 7.0. Once dissolved, 100 mg NH_2-SBA-15 silica were added to 10 mL of this solution. Catalytic activity of the protein solution before immobilization was measured using *p*-nitrophenyl acetate (*p*NP-acetate) as substrate as described previously [52]. Immobilization was allowed to proceed at different intervals after which the catalytic activity was evaluated in the supernatant and on the mesoporous silica (prior re-suspension in HEPES (40 mM, pH 7.0)) previously separated by centrifugation (13000 rpm, room temperature, 1.5 min), and compared to the activity of the initial esterase solution. The immobilization proceeded until the activity of the supernatant was constant, which indicated full enzyme immobilization. Then, the suspension was filtered using sintered glass funnel, washed with HEPES (40 mM, pH 7.0), and vacuum-dried. The specific activity of the immobilized enzyme was evaluated by quantifying the total units of esterase activity (measured using *p*NP-acetate as substrate) at the beginning of the experiment and the total units of the immobilized biocatalyst (tested using 9.4 mg of the biocatalyst re-suspended in 1 mL HEPES buffer, pH 7.0), as reported previously [52]. Under these conditions, after 48 h, only 4% of the initial activity remained in the supernatant and the enzyme loading obtained was of 48 mg esterase per gram of NH_2-SBA-15 (or 96% total protein being immobilized) after calculation of protein concentrations according to Bradford assay with bovine serum albumin as the standard [56].

Fig. 4 summarizes the protocol used for the synthesis of the mesostructured silica support and EH1 immobilization, performed at pH 7.0, at which the amino groups of the support are positively charged and the net charge of the enzyme is negative. Additional comments on enzyme immobilization kinetics is provided in the Supporting Information.

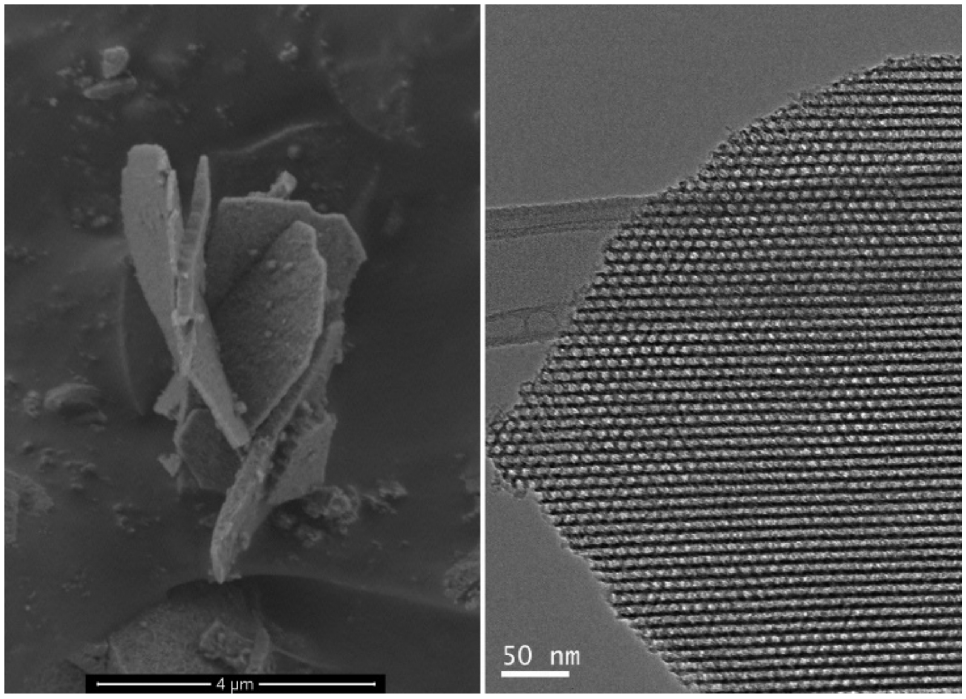

Fig. 2. Left: SEM micrograph showing the plate-like morphology of SBA-15 silica particles. Right: TEM image recorded in the direction of the axis of SBA-15 mesopore channels. For experimental details see Experimental Section.

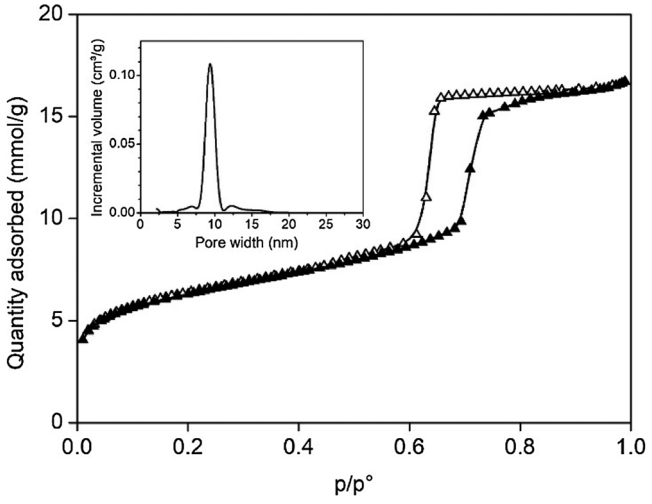

Fig. 3. Nitrogen adsorption-desorption isotherm at 77 K of silica SBA-15. Full symbols correspond to the adsorption branch and empty symbols to desorption. The inset shows the pore-size distribution calculated by NLDFT. The Nitrogen adsorption-desorption isotherm for NH_2-SBA-15 is not shown but it is estimated that the grafting of aminopropyl groups on the surface of pores will decrease the pore width by ca. 2 nm.

2.4. EH1 immobilization on magnetic microparticles

Two types of commercial (PerkenElmer LAS, Rodgau, Germany) magnetic microparticles with differentiated structural, chemical and physical properties were used for surface immobilization of the enzyme. The first one is based on a *N*-hydroxysuccinimidyl (NHS) ester modified polyvinyl alcohol (PVA) network with embedded magnetite (M) (http://www.chemagen.com/magneticbeads.html) with a diameter size range of 1–5 µm. The polymeric shell is chemically modified with the iminodiacetic acid (IDA) tridentate ligand, which is eventually used for enzyme immobilization. These beads, herein referred to as M-PVA-IDA@Ni, were activated with $NiSO_4$ prior to being used to capture His-tagged proteins. The second type of microparticles, referred to as M-Ag-NTA@Ni, is fabricated by coating a ferromagnetic core with 6% of crosslinked agarose (http://www.cube-biotech.com/s-products/magnetic-beads/his-affinity-magbeads/ni-nta-magbeads). These ready-to-use Ni-activated particles possess significantly larger dimensions (25–30 µm), and bear nitrilotetracetic acid (NTA) tetradentate ligand as chelating agent instead of IDA. The characteristics of the magnetic particles, which are commercially available, are described in https://cube-biotech.com/his-affinity-purification-guide. The particles are Ni^{2+}-activated and thus can be used for protein purification given the affinity for hexahistidine-tags. In our study we used these carriers for site-directed immobilization by capturing His-tagged proteins though Ni^{2+} which is differentially incorporated to the particles, as described above. We would like to mention that after immobilization via the hexahistidine-tags, it is possible that other groups others than His interact with the metal, or that some ion exchange may occur. The same enzyme immobilization protocol was used for both sorts of supports. Shortly, particles (50 µL; delivered as 25% particle suspensions) were retained by a magnet and the solution was decanted; after a careful removal of the supernatant the pellet was washed twice with sodium phosphate buffer (30 mM, pH 8.0) and mixed afterwards with the enzyme solution (600 µL, 1.0 mg mL^{-1}) in the same buffer. Microparticles were stirred until they were fully suspended. Upon incubation for 2 h at room temperature, the particles were once again retained by a magnet and the solution decanted and washed by repeating the procedure described above 3 times. Final enzyme-particle conjugates were suspended in 200 µL of sodium phosphate buffer (30 mM, pH 8.0) buffer and used directly for activity measurements. Protein loading was calculated by measuring the difference in protein concentration before and after the immobilization experiment. Hence, protein concentrations of $\approx$ 0.64 g L^{-1} (or $\approx$ 10.2 µg g^{-1}) for M-PVA-IDA@Ni and $\approx$ 0.52 g L^{-1} (or $\approx$ 8.3 µg g^{-1}) for M-Ag-NTA@Ni were measured.

Fig. 5 summarizes the protocol used for EH1 immobilization on magnetic microparticles. The EH1 employed was initially designed with a His-tag for purification purposes and could therefore be directly employed for immobilization.

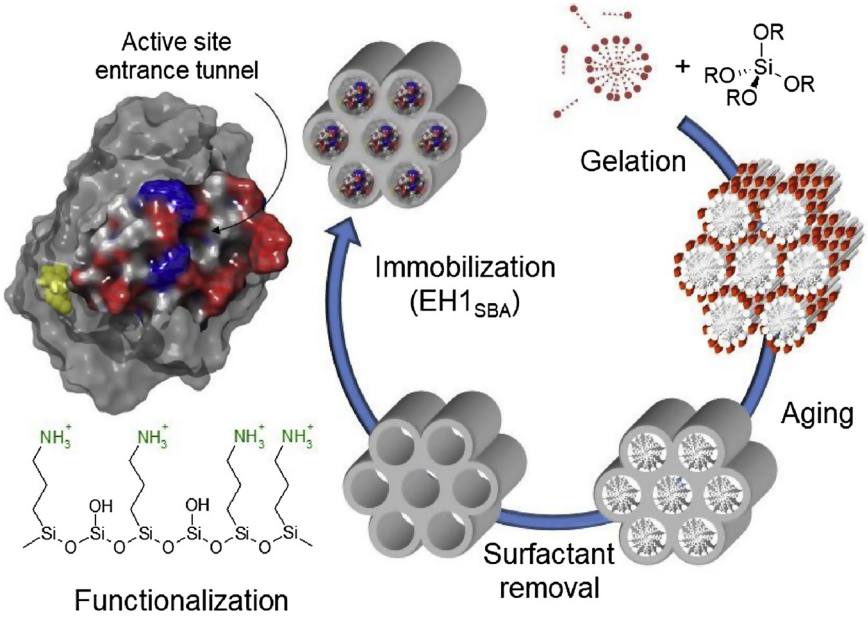

Fig. 4. Schematic representation of the protocol used for the synthesis of the NH2-SBA-15 mesostructured silica support and EH1 immobilization. EH1 structure with the cavity electrostatic surface, in red the negative charge and in blue the positive charge, created with Maestro, is represented. The access to the active site tunnel is indicated with an arrow. The position of the Hig6-tag is highlighted in yellow. Note that only one enzyme biomolecule is visible in the entrance of the pores, but each cylindrical pore channel could accommodate on average 26 enzyme molecules arranged in a row along the channel.

2.5. Ester bond hydrolysis activity assessment

Hydrolytic activity of free and immobilized preparations was assayed using a pH indicator assay at 550 nm using 96 structurally diverse esters in 384-well plates as previously described [51,52]. Briefly, reactions (total volume of 44 µL) were performed in 5 mM N-(2-hydroxyethyl)piperazine-N'-(3-propanesulfonic acid) buffer (pH 8.0) containing 1.14 mg mL^{-1} of each ester and 0.45 mM phenol red (used as pH indicator), and 2 µL of immobilized preparation (from a 10 mg solid particle per mL in 40 mM HEPES buffer pH 7.0) or free enzyme solution (1 mg mL^{-1}) were immediately added to each well using an Eppendorf Repeater M4 pipette (Eppendorf, Hamburg, Germany). The total reaction volume was 44 µL. Note that a fixed concentration of 1.14 mg mL^{-1} of each ester was used; this corresponds to an ester concentration ranging from 1.28 to 13.2 mM, depending on the ester [51], concentrations that in all cases were above the K_m values for the target enzyme [51], so that the substrate saturation was guarantee for activity tests. After incubation at 30 °C and 150 rpm in a Synergy HT Multi-Mode Microplate Reader, ester hydrolysis was measured spectrophotometrically in continuous mode at 550 nm over 24 h. One unit (U) of enzyme activity was defined as the amount of free enzyme or enzyme bound to the carrier required to transform 1 µmol of substrate in 1 min under the assay conditions using the reported extinction coefficient (εPhenol red at 550 nm = 8450 M^{-1} cm^{-1}) [51,52]. All values were corrected for non-enzymatic transformation using as controls the suspensions of the mesostructured silica and magnetic microparticles without immobilized enzyme. Note that, using those control materials, no appreciable (below detection limit; see [51]) hydrolysis was detected for any of the tested esters.

The assay used to determine the substrate specificity and enantiospecificity is pH-based, which means that the pH of the reaction solution changes as the substrates are hydrolyzed. As the immobilization strategies are sensitive towards pH, we determined the pH change during the course of the reactions to evaluate the risk of enzyme

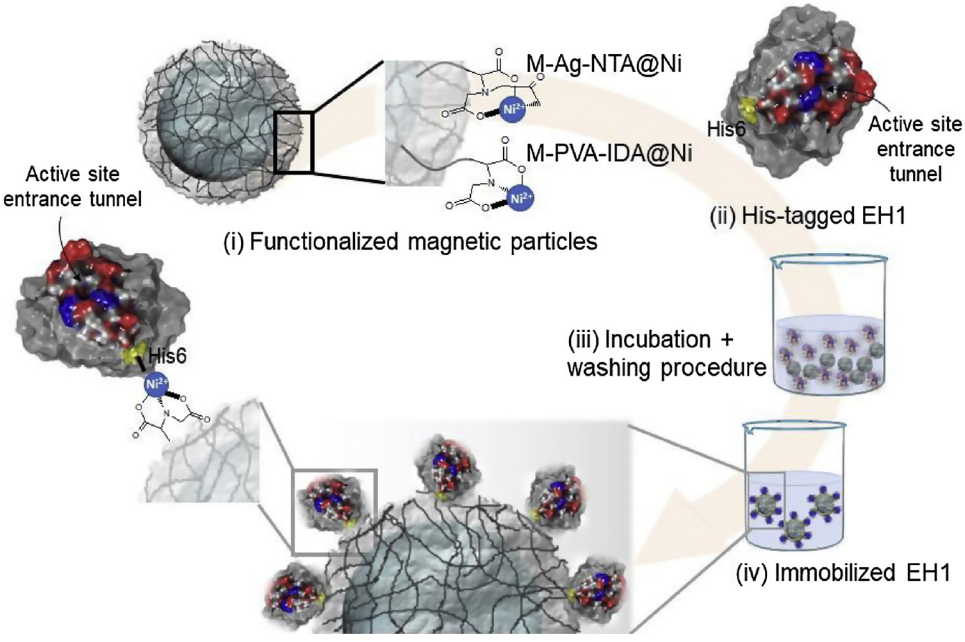

Fig. 5. Schematic representation of the protocol used for the immobilization of EH1 on two types of magnetic microparticles with different chemical and physical properties, namely, agarose-coated ferromagnetic core-shell microparticles in which EH1 was attached through a NTA linker and polyvinyl alcohol particles embedded with magnetite and grafted with an IDA linker. By using Maestro, the position of the hexahistidine-tag in EH1 is highlighted in yellow, in blue (positive charge) and red (negative charge) the residues conforming the entrance to the active site, and in grey color the rest of the protein. The access to the active site tunnel is indicated with an arrow.

leakage through pH change during the course of the reaction. Additional details on the evaluation of pH change before, during and after activity tests and their possible effect of enzyme leaching from the carriers, which was found below detection limit, are given in the Supporting Information.

2.6. Structure analysis

The crystal structure of EH1 protein was recently solved and X-ray diffraction data collection and refinement statistics are available [51]. The Maestro interface (version 10.4) was used to provide structural analysis.

3. Results and discussion

3.1. Substrate profile and enantiospecificity of EH1 immobilized in NH_2-SBA-15

EH1, which was used as model enzyme was immobilized on the amino-functionalized ordered mesoporous material NH_2-SBA-15 (see Experimental section and Fig. 4). The immobilized preparation, with enzyme loads (48 mg protein per gram of silica) in the range of previously reported studies [19,20], will be referred to as $EH1_{SBA}$. The hydrolytic activity of $EH1_{SBA}$ was evaluated relative to a set of 72 esters hydrolyzed by free EH1 (see Experimental section). The immobilization caused a significant reduction in the substrate range (Fig. 6; Table S1) as $EH1_{SBA}$ was only able to hydrolyze 17 esters, with cyclohexyl butyrate being the preferred substrate (5.3 ± 0.02 U mg^{-1}). Thus, the immobilization of the enzyme inside pores narrows the substrate scope. Most likely, this significant reduction of substrates may be a consequence of the hydrophilic surface chemistry of the functionalized mesoporous silica and of the limited access of molecules to the active site when the enzyme is immobilized inside the pores, as it has been previously observed for other enzymes [46,47]. However, the fact that $EH1_{SBA}$ efficiently hydrolyzed large molecules such as phenyl acetate and phenyl propionate, vinyl benzoate, benzyl 2-hydroxy-3-phenylpropionate, benzoic acid 4-formyl-phenylmethyl ester, 1-naphthyl acetate, 1-naphthyl butyrate, and triglycerides (Fig. 6), suggests further factors contributing to the substrate spectra of the final enzymatic preparation. Indeed, the partitioning coefficient (LogP value) and the molecular volume, which reflects electronic and steric effects and hydrophobic and hydrophilic characteristics, revealed that esters being hydrolyzed by $EH1_{SBA}$ ranged from LogP values of −0.19 to 3.85, and molecular volumes of 115.37 to 297.46 $Å^3$, respectively. However, many other esters with similar values were not accepted as substrates (Fig. 6; Table S1). Even very hydrophilic and small esters such as Υ-valerolactone (LogP: −0.27; volume: 96.74 $Å^3$) and methyl lactate (LogP: −0.72; volume: 98.57 $Å^3$) were not hydrolyzed.

Focusing on stereochemistry, EH1 was capable of hydrolyzing 14 chiral esters, that is, (*R*) and (*S*) enantiomers of menthyl acetate, methyl mandelate, ethyl 4-chloro-3-hydroxybutyrate, methyl 3-hydroxybutyrate, methyl 3-hydroxyvalerate, methyl lactate and ethyl lactate (Fig. 6; Table S1). The E_{app} for the free EH1, calculated as the ratio of specific activity (U mg^{-1}) of the preferred chiral ester over that of the non-preferred one when both esters were tested separately [53,54], ranged from 1.45 to 14.2 (Table 1). $EH1_{SBA}$ was capable of hydrolyzing only 4 out of the 14 chiral esters for which the free EH1 showed activity. Interestingly, the E_{app} for ethyl (*R*)-4-chloro-3-hydroxybutyrate over ethyl (*S*)-4-chloro-3-hydroxybutyrate (LogP: 0.33; volume: 145.95 $Å^3$) increased from 1.45 for EH1 to 419 for $EH1_{SBA}$. Slight increase in the E_{app} (2.6 vs 4.7 in the same order) was observed for ethyl (*R/S*)-lactate (LogP: -0.19; volume: 115.37 $Å^3$) (Table 1). Other chiral esters with lower or higher LogP values and molecular volumes were not accepted as substrates.

To conclude, the immobilization in NH_2-SBA-15 caused not only a significant reduction of the substrate spectrum but also a significant increase in E_{app}, particularly for ethyl (*R*)-4-chloro-3-hydroxybutyrate, a chiral compound broadly appreciated for the synthesis of biologically and pharmacologically important materials such as (*R*)-carnitine, (*R*)-4-amino-3-hydroxybutyric acid, and (*R*)-4-hydroxy-2-pyrrolidone [61]. We further evaluated whether the observed changes in specificity and E_{app} of EH1 induced by the immobilization in NH_2-SBA-15 were specific or not for this support. Therefore, we immobilized EH1 on other carriers, i.e., magnetic microparticles, where the enzyme was chemically

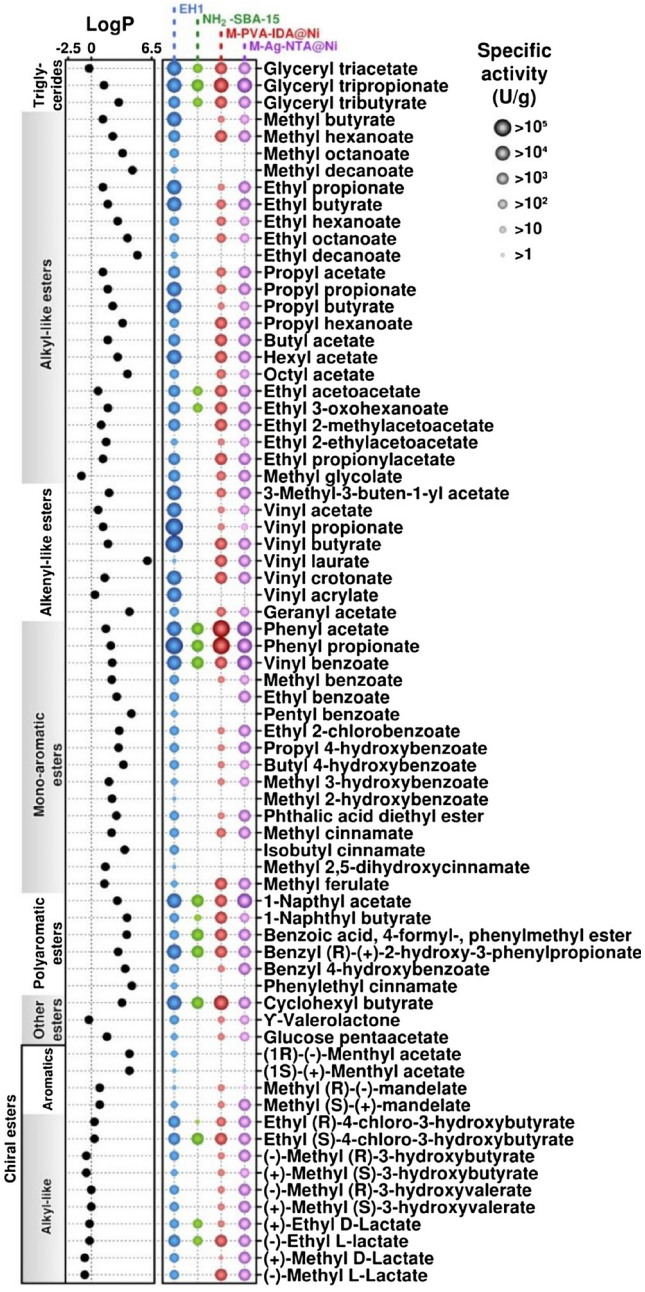

Fig. 6. Substrate range of free EH1 and its immobilized preparations. The ID code representing each variant is color coded. This Figure is created from data given in Supporting Table S1. The classes of esters tested are indicated on the left side. The Figure was created with the R language console using information about the specific activity (units g^{-1}) of the analyzed enzymes against the 72 substrates hydrolyzed by EH1 as a starting point. The activity protocol established and used to identify the esters hydrolyzed by each EH1 variant was based on a continuous pH indicator assay at pH 8.0 and 30 °C, performed in triplicate and corrected for background signal (see Experimental section). The LogP values for each ester were calculated using the ACD/ChemSketch 2015.2.5 software.

Table 1
Enantiospecificity of EH1 and immobilized preparations against a number of chiral esters, as revealed by calculations of E_{app}.

Ester[a]	Estimated E_{app}[b]			
	EH1	$EH1_{SBA}$	$EH1_{IDA}$	$EH1_{NTA}$
1**RS**	9.65 ± 0.70	n.d	n.d	n.d
2**RS**	14.2 ± 0.46	n.d	0.95 ± 0.20	151 ± 1
3**RS**	1.45 ± 0.05	419 ± 9	3.58 ± 0.03	0.64 ± 0.24
4**RS**	4.89 ± 0.36	n.d	9.09 ± 0.20	3.16 ± 0.31
5R**S**	4.41 ± 0.04	n.d	3.12 ± 0.07	1.58 ± 0.29
6R**S**	2.60 ± 0.03	4.73 ± 0.17	154 ± 9	2.02 ± 0.17
7R**S**	4.56 ± 0.36	n.d	194 ± 2	1.45 ± 0.19

[a] Compounds ID: 1RS, (*R/S*)-menthyl acetate; 2RS: methyl (*R/S*)-mandelate; 3RS: ethyl (*R/S*)-4-chloro-3-hydroxybutyrate; 4RS: methyl (*R/S*)-3-hydroxybutyrate; 5RS: methyl (*R/S*)-3-hydroxyvalerate; 6RS: ethyl (*R/S*)-lactate; 7RS: methyl (*R/S*)-lactate; the preferred chiral ester is indicated **underlined and in bold**.

[b] E_{app} was calculated per each of the pairs of enantiomers as the ratio of specific activity (U mg^{-1}) per each of the 14 chiral esters when pure stereoisomers were tested separately, as described elsewhere [53,54]. These calculations were extracted from data in Table S1. n.d.: Activity not detected under our assay conditions.

linked to the surface of the support. Other carriers such as Celite® and Sepabeads were used but the resulting preparations showed residual activity and thus were not further considered in this study.

3.2. Substrate profile and enantiospecificity of EH1 immobilized on magnetic microparticles

EH1 was immobilized on two types of magnetic microparticles (see Experimental section), namely, agarose-coated core-shell ferromagnetic particles to which EH1 was attached through a NTA linker (referred to as $EH1_{NTA}$; Fig. 4), and PVA particles with embedded magnetite and grafted with an IDA linker (referred to as $EH1_{IDA}$; Fig. 5).

$EH1_{IDA}$ preparation has the ability to hydrolyze 60 substrates, with phenyl acetate being the preferred ester (104.0 ± 0.13 U mg^{-1}) (Fig. 6; Table S1). $EH1_{NTA}$ hydrolyzed the same set of 60 substrates hydrolyzed by $EH1_{IDA}$ plus ethyl benzoate, with also phenyl acetate being the preferred ester (90.5 ± 1.8 U mg^{-1}). Compared to the free enzyme these preparations were unable to hydrolyze 11 esters, which included methyl octanoate, methyl decanoate, ethyl decanoate, pentyl benzoate, methyl 2-hydroxybutyrate, isobutyl cinnamate, phenethyl cinnamate, isobutyl cinnamate, methyl 2,5-dihydroxycinnamate, menthyl acetate, and vinyl acrylate. None of these 11 esters were either hydrolyzed by $EH1_{SBA}$. All but vinyl acrylate (LogP: 0.38; volume: 96.07 $Å^3$) could be considered as large hydrophobic esters (LogP: from 1.51 to 4.96; volume: from 136.59 to 244.4 $Å^3$). However, other large molecules with LogP values as high as 3.64 such as benzyl 4-hydroxybenzoate, and molecular volume as high as 338.38 $Å^3$ such as glucose pentaacetate, were hydrolyzed, suggesting again that factors others than surface chemistry and substrate access limitations may contribute to the substrate spectra of the final enzymatic preparations $EH1_{NTA}$ or $EH1_{IDA}$. Following on from this, it should be mentioned that both preparations showed similar substrate spectra, with a clear distinct preference for alkyl esters. Indeed, whereas $EH1_{NTA}$ showed from 3 to 19-fold higher preference for short alkyl esters such as methyl butyrate, ethyl propionate, ethyl butyrate, propyl acetate, propyl propionate, propyl butyrate, and butyl acetate, $EH1_{IDA}$ preferred (from 1.4 to 5-fold) longer esters such as methyl hexanoate, ethyl hexanoate, ethyl octanoate, hexyl acetate, and octyl acetate (Table S1).

All esters hydrolyzed by $EH1_{SBA}$ were also hydrolyzed by $EH1_{IDA}$ and $EH1_{NTA}$, whereas the immobilization on the surface of magnetic microparticles produced biocatalysts capable of converting 44 esters which $EH1_{SBA}$ did not accept. These range from small hydrophilic esters such as methyl glycolate (LogP: -1.07; volume: 81.98 $Å^3$) to large hydrophobic esters such as vinyl laurate (LogP: 6.04; volume: 252.91 $Å^3$).

With regards to stereochemistry, $EH1_{IDA}$ catalyzed the hydrolysis of all those chiral esters hydrolyzed by the free enzyme except (*R*)-(-)-menthyl acetate and (*S*)-(+)-menthyl acetate, which were not accepted as substrates (Fig. 6; Table S1). Interestingly, the E_{app} for (-)-methyl (*S*)-lactate over (+)-methyl (*R*)-lactate increased from ~4.6 for the free enzyme to ~194 for $EH1_{IDA}$ (Table 1). Similarly, the E_{app} for (-)-ethyl (*S*)-lactate over (+)-ethyl (*R*)-lactate increased from ~2.6 to ~154, in the same order. No significant changes of the E_{app} were observed for the other chiral esters, including ethyl (*R/S*)-4-chloro-3-hydroxybutyrate for which the E_{app} significantly increased after immobilization in NH_2-SBA-15. $EH1_{NTA}$ was capable of hydrolyzing the same set of chiral esters as $EH1_{IDA}$ (Fig. 4; Table S1), but a notable difference was observed. Particularly, the E_{app} for methyl (*S*)-(+)-mandelate over methyl (*R*)-(-)-mandelate increased from ~14.2 for the free enzyme to ~150 for the $EH1_{NTA}$ preparation (Table 1), substrates for which $EH1_{IDA}$ did not show any preference (E_{app} approx. 1). No significant changes of the E_{app} were observed for the other chiral esters.

In summary, immobilization on the surface of agarose-coated large core-shell ferromagnetic microparticles (25–30 μm) through a NTA linker slightly altered the substrate range (61 esters) while producing a biocatalyst more selective for short alkyl esters and for methyl (*S*)-(+)-mandelate. Moreover, immobilization on the surface of small polyvinyl alcohol magnetic microparticles (1–5 μm) through an IDA linker also slightly altered the substrate range (60 esters) while producing a more selective biocatalyst for ethyl and methyl (*S*)-lactate and slight preference for longer alkyl esters.

3.3. Flexibility constrains as determinants defining chiral preference of biocatalysts

Based on the crystal packing (PDB 5JD4) EH1 is a dimer [51], the dimensions of that are approximately 70 Å × 44 Å × 42 Å (or 7 nm × 4.4 nm × 4.2 nm). Enzymes with these dimensions have been successfully immobilized in large-pore size SBA-15 materials [38]. The mesoporous silica used to immobilize EH1 possesses pore channels which are about 200 nm long with a highly uniform diameter close to 9.3 nm (Figs. 2 and 3). The grafting of aminopropyl groups on the surface of pores makes the actual pore width available for enzyme immobilization even slightly smaller (ca. 2 nm). Therefore, it is expected that the cylindrical pore channels may accommodate only one enzyme molecule along the channel diameter. Considering the enzyme diameter (about 7 nm × 4.4 nm × 4.2 nm) and the length (200 nm) and diameter (9.3 nm for SAB-15 or ca. 7.3 nm for the amino funcionalized material) of the channels, it follows that each cylindrical pore channel could accommodate on average 26 enzyme molecules arranged in a row along the channel, in which each enzyme molecule may have restricted movement due to the similar size of enzyme structure and pores. Hence, there will be very little space for substrate and product molecules to diffuse in and out of the channels. Additional details on the enzyme load and enzyme immobilization kinetics in the NH_2-SBA-15 support are given in the Supporting Information.

To investigate which zones of the negatively charged proteins may most likely interact with the positively charged surface of the pores, a surface electrostatic analysis of the EH1 structure was performed. The analysis shows a negative zone around the binding cavity entrance (Fig. 4), and thus it is plausible that the active site is oriented to the surface of the amino-functionalized ordered mesoporous material. The hindered movement of the enzyme inside the pores and the most likely unfavorable orientation of the EH1 binding cavity may explain the restricted substrate spectrum of the $EH1_{SBA}$ preparation. However, both reasons per se do not explain the fact that the enzyme immobilized inside the 7.3 nm diameter pores of NH_2-SBA-15 materials retains the capacity to hydrolyze some very large and hydrophobic molecules such

as benzoic acid 4-formyl-phenylmethyl ester, while being unable to hydrolyze very small esters such as vinyl acetate (Fig. 6). It is plausible that factors others than access of molecules to the pores and to the active site play an additional role in determining the substrate specificity (including enantiospecificity). In this study we hypothesized that protein immobilization could affect not only the free movement of the enzyme but also impose flexibility constraints to the enzyme molecule. Note that catalytic triads in serine ester hydrolases are located in a catalytic environment where residues lining the active site are contributing to binding and correct positioning of substrates [51,52]. Altering the position, distances and angles of those residues may alter the binding capacity. This may explain the binding preference of $EH1_{SBA}$ for ethyl (*R*)-(-)-4-chloro-3-hydroxybutyrate over (*S*)-(+)-4-chloro-3-hydroxybutyrate.

To prove whether the flexibility constraints may explain the improved E_{app} for ethyl (*R*)-(-)-4-chloro-3-hydroxybutyrate, EH1 was immobilized in NH_2-SBA-15 materials with same surface chemistry (1.6 or 1.4 mmol aminopropyl groups per gram of support) but wider pores (pore diameter of 16.7 or 14.0 nm) (details on the synthesis and characterization of these supports are given in the Supporting Information). The specific activity of both preparations towards ethyl (*R*/*S*)-(-/+)-4-chloro-3-hydroxybutyrate was determined, and the E_{app} calculated. The E_{app} for EH1 immobilized in the material with a diameter of 16.7 nm was found to be 4.51 (*R* preference), and 4.57 (*R* preference) for that with 14.0 nm diameter. This value is slightly higher than that of the free enzyme (~1.5) but significantly lower than that obtained when the enzyme was immobilized in the material with pores of 9.3 nm diameter (~420) where EH1 has a tight fit. These results suggest that restricting the enzyme movement and/or promoting enzyme rigidity by non-covalent enzyme immobilization in pores with diameters close to that of the enzyme crystal packing may help promoting enantiospecificity.

In $EH1_{NTA}$ and $EH1_{IDA}$ a controlled immobilization via His-tag is used. Immobilization of proteins through the His-tag allows an oriented immobilization of all enzyme molecules, which is important to have a clue about the accessibility of the active site cavity with respect to the surface of the support. In this line, immobilization of the His-tagged enzyme onto nickel(II)-cyclam grafted mesoporous silica have been shown to allow tailored made adsorption [62] as this may avoid problems associated to an unfavourable orientation of the enzyme. An analysis of the EH1 structure revealed that orientation of EH1 both in $EH1_{NTA}$ and $EH1_{IDA}$ is favorable for the substrate access to the active site tunnel. Indeed, the *N*-terminus of the enzyme where the His-tag is located is oriented opposite to the active site cavity (Fig. 5). However, this favorable orientation, which may occur in both preparations, does not explain per se why the two immobilized preparations were not able to hydrolyze 12 ($EH1_{NTA}$) and 11 ($EH1_{IDA}$) esters which were hydrolyzed by the free enzyme. These molecules included large esters such as methyl octanoate, methyl decanoate, ethyl decanote, pentyl benzoate, methyl-2-hydroxybenzoate, isobutyl cinnamate, methyl 2,5-dihydroxycinnamate, phenylethyl cinnamate, and menthyl acetate, but also short esters such as vinyl acrylate, which a priori should cause less diffusional problems compared to larger esters. Also, it does not explain that both preparations were able to hydrolyze methyl benzoate (LogP: 2.2; volume: 263.3 $Å^3$) and vinyl benzoate (LogP: 2.25; 139.74 $Å^3$), whereas the slightly larger ethyl benzoate (LogP: 2.73; 145.38 $Å^3$) was only accepted by $EH1_{NTA}$ (Fig. 6; Table S1). Finally, it does not explain the increased preference of $EH1_{NTA}$ for methyl (*S*)-(+)-mandelate (LogP: 0.9; 153.42 $Å^3$) or the increased preference of $EH1_{IDA}$ for ethyl (*S*)-lactate (LogP: -0.72; 98.57 $Å^3$) and larger alkyl esters. We hypothesize that the stronger interaction of the protein through a NTA linker in $EH1_{NTA}$ compared to IDA linker in $EH1_{IDA}$ may slightly increase the rigidity of the protein and thus alter the entrance or positioning of a specific subset of esters, thus influencing substrate preference and specificity for specific set of esters, including chiral esters. It is also plausible that the smaller particles may have a higher density of proteins, which may affect their packing on the surface.

4. Conclusion

In this manuscript we studied the effect of immobilization of a model enzyme in an unprecedented manner. Through an extensive analysis of the substrate spectra, we examined in depth the contribution of surface chemistry, particle size, substrate accessibility to the active site tunnel, and flexibility constraints, driven by each immobilization strategy, on enzyme substrate specificity and stereochemistry. We found that flexibility constraints, which can be modulated through careful materials design (particle size, pore size and architecture) and functionalization (strength of the linkage), are among the most important factors determining the specificity and stereochemistry of immobilized enzymes. These constraints may most likely affect the enzyme structure and the active site configuration and in turn the access and positioning of substrates in the active site. This was herein proven by converting an ester hydrolase with broad substrate spectrum but non-enantiospecific, a common feature in natural esterases, into biocatalysts capable of converting specific molecules, including stereoisomers, depending on the immobilization strategy applied. Therefore, by controlling the immobilization strategy, the size and the functionalization of materials and interfaces employed, one can use substrate promiscuous enzymes to design biocatalysts for multiple selective catalytic routes and stereochemistry, and to produce a range of chiral molecules which are important building blocks for drug/fragrance discovery, chemical biology, and modern materials science. Finally, the present study suggests that a controlled manipulation of specificity of enzymes can be achieved to a higher extent than previously envisaged by size/chemistry-tunable materials, to produce more efficient catalysts. Studying mesoporous materials with a large constellation of pore sizes and materials with different density of reactive groups may be of interest in the future to obtain a clue about their impact in enzyme rigidity/flexibility and to design carriers with characteristics capable of producing a desired change in substrate specificity or stereochemistry. Investigation of immobilization effect by computational methods will help deepening into the structural constrains induced by different carriers, the quantification of the rigidity/flexibility, and its link with specificity (see additional comments in Supporting Results).

Acknowledgements

This project received funding from the European Union's Horizon 2020 research and innovation program Blue Growth: Unlockingthe potential of Seas and Oceans under grant agreement no. 634486 (project acronym INMARE). This research was also supported by the grants PCIN-2014-107 (within ERA NET IB2 grant nr. ERA-IB-14-030 - MetaCat), PCIN-2017-078 (within the ERA-MarineBiotech grant ProBone), BIO2014-54494-R, MAT2016-77496-R, BIO2017-85522-R, and CTQ2016-79138-R from the Spanish Ministry of Economy, Industry and Competitiveness. A.B. acknowledges the support from the Spanish Ministry of Economy, Industry and Competitiveness (MAT2017-88808-R grant), María de Maeztu Units of Excellence Programme (MDM-2016-0618), and the Diputación de Guipúzcoa for current funding in the frame of Gipuzkoa Fellows program. G.D. thanks the German Federal Ministry of Education and Research (BMBF, Grant No. 031A095C) for funding in the frame of the Molecular Interaction Engineering program (Biotechnologie 2020+). The authors gratefully acknowledge financial support provided by the European Regional Development Fund (ERDF). C.C. thanks the Spanish Ministry of Economy, Industry and Competitiveness for a PhD fellowship (Grant BES-2015-073829).

Appendix A. Supplementary data

Supplementary material related to this article can be found, in the online version, at doi: https://doi.org/10.1016/j.apcata.2018.08.003.

References

[1] D.N. Tran, Jr.K.J. Balkus, ACS Catal. 1 (2011) 956–968.
[2] A.S. Bommarius, M.F. Paye, Chem. Soc. Rev. 42 (2013) 6534–6565.
[3] G. Kde, R. Daiha, S.D. Angeli, R.V. de Oliveira, Almeida, PLoS ONE 10 (2015) e0131624.
[4] F. Jia, B. Narasimhan, S. Mallapragada, Biotechnol. Bioeng. 111 (2014) 209–222.
[5] Z. Zhou, M. Hartmann, Chem. Soc. Rev. 42 (2013) 3894–3912.
[6] E.P. Cipolatti, A. Valério, R.O. Henriques, D.E. Moritz, J.L. Ninow, D.M.G. Freire, E.A. Manoel, R. Fernandez-Lafuente, D. De Oliveira, RSC Adv. 6 (2016) 104675–104692.
[7] H.R. Luckarift, J.C. Spain, R.R. Naik, M.O. Stone, Nat. Biotechnol. 22 (2004) 211–213.
[8] S.-H. Jun, J. Lee, B.C. Kim, J.E. Lee, J. Joo, H. Park, J.H. Lee, S.-M. Lee, D. Lee, S. Kim, Y.-M. Koo, C.H. Shin, S.W. Kim, T. Hyeon, J. Kim, Chem. Mater. 24 (2012) 924–929.
[9] N. Brun, A. Babeau Garcia, H. Deleuze, M.-F. Achard, C. Sanchez, F. Durand, V. Oestreicher, R. Backov, Chem. Mater. 22 (2010) 4555–4562.
[10] M. Sevilla, T. Valdés-Solís, P. Tartaj, A.B. Fuertes, J. Colloid Interface Sci. 340 (2009) 230–236.
[11] M.I. Shukoor, F. Natalio, H.A. Therese, M.N. Tahir, V. Ksenofontov, M. Panthöfer, M. Eberhardt, P. Theato, H.C. Schröder, W.E.G. Müller, W. Tremel, Chem. Mater. 20 (2008) 3567–3573.
[12] H. Gustafsson, A. Küchler, K. Holmberg, P. Walde, J. Mater. Chem. B Mater. Biol. Med. 3 (2015) 6174–6184.
[13] P.B. Messersmith, M. Textor, Nat. Nanotechnol. 2 (2007) 138–139.
[14] Z.D. Knežević-Jugović, M.G. Žuža, S.M. Jakovetić, A.B. Stefanović, E.S. Džunuzović, K.B. Jeremić, S.M. Jovanović, Biotechnol. Prog. 32 (2016) 43–53.
[15] J. Britton, C.L. Raston, G.A. Weiss, Chem. Commun. 52 (2016) 10159–10162.
[16] E. Zare-Eelanjegh, D.K. Bora, P. Rupper, K. Schrantz, L. Thöny-Meyer, K. Maniura-Weber, M. Richter, G. Faccio, ACS Appl. Mater. Interfaces 8 (2016) 20432–20439.
[17] A. Rao, A. Bankar, A. Shinde, A.R. Kumar, S. Gosavi, S. Zinjarde, ACS Appl. Mater. Interfaces 4 (2012) 871–877.
[18] M.P. Conte, K.H. Lau, R.V. Ulijn, ACS Appl. Mater. Interfaces 9 (2017) 3266–3271.
[19] E. Magner, Chem. Soc. Rev. 42 (2013) 6213–6266.
[20] V. Gascón, I. Díaz, C. Márquez-Álvarez, R.M. Blanco, Molecules 19 (2014) 7057–7071.
[21] V. Gascón, C. Márquez-Álvarez, R.M. Blanco, Appl. Catal A: General 482 (2014) 116–126.
[22] A. Küchler, M. Yoshimoto, S. Luginbühl, F. Mavelli, P. Walde, Nat. Nanotechnol. 11 (2016) 409–420.
[23] E. Serra, A. Mayoral, Y. Sakamoto, R.M. Blanco, I. Díaz, Microporous Mesoporous Mater. 114 (2008) 201.
[24] J. Fan, W. Shui, P. Yang, X. Wang, Y. Xu, H. Wang, X. Chen, D. Zhao, Chemistry 11 (2005) 5391–5396.
[25] S. Hudson, E. Magner, J. Cooney, B.K. Hodnett, J. Phys. Chem. B 109 (2005) 19496–19506.
[26] J. He, Y. Xu, H. Ma, Q. Zhang, D.G. Evans, X. Duan, J. Colloid Interface Sci. 298 (2006) 780–786.
[27] D. Jung, C. Streb, M. Hartmann, Int. J. Mol. Sci. 11 (2010) 762–778.
[28] M. Vittorini, E. Dumitriu, G. Barletta, F. Secundo, Bioprocess Biosyst. Eng. 34 (2011) 247–251.
[29] J.M. Gómez, M.D. Romero, T.M. Fernández, E. Díez, Bioprocess Biosyst. Eng. 35 (2012) 1399–1405.
[30] M.M. Wan, W.G. Lin, L. Gao, H.C. Gu, J.H. Zhu, J. Colloid Interface Sci. 377 (2012) 497–503.
[31] H. Zhang, E. Xun, J. Wang, G. Chen, T. Cheng, Z. Wang, T. Ji, L. Wang, Int. J. Mol. Sci. 13 (2012) 5998–6008.
[32] N. Canilho, J. Jacoby, A. Pasc, C. Carteret, F. Dupire, M.J. Stébé, J.L. Blin, Colloids Surf. B Biointerfaces 112 (2013) 139–145.
[33] S. Li, Z. Wu, M. Lu, Z. Wang, Z. Li, Molecules 18 (2013) 1138–1149.
[34] P. Bhange, N. Sridevi, D.S. Bhange, A. Prabhune, V. Ramaswamy, Int. J. Biol. Macromol. 63 (2014) 218–224.
[35] G. Chandrasekar, M. Hartmann, V. Murugesan, J. Nanosci. Nanotechnol. 14 (2014) 2606–2613.
[36] A. Kumari, B. Kaur, R. Srivastava, R.S. Sangwan, Biochem. Biophys. Rep. 2 (2015) 108–114.
[37] P. Ramachandran, G.K. Narayanan, S. Gandhi, S. Sethuraman, U.M. Krishnan, Appl. Biochem. Biotechnol. 175 (2015) 2332–2346.
[38] J.M. Bolivar, V. Gascon, C. Marquez-Alvarez, R.M. Blanco, B. Nidetzky, Langmuir 33 (2017) 5065–5076.
[39] P. Corell Escuin, A. García-Bennett, J.V. Ros-Lis, A. Argüelles Foix, A. Andrés, Food Chem. 217 (2017) 360–363.
[40] X. Fan, W. Liang, Y. Li, H. Li, X. Liu, Microb. Cell Fact. 16 (2017) 149.
[41] S. Hüttner, M. Zezzi Do Valle Gomes, L. Iancu, A. Palmqvist, L. Olsson, Bioresour. Technol. 239 (2017) 57–65.
[42] A. Vinu, N. Gokulakrishnan, V.V. Balasubramanian, S. Alam, M.P. Kapoor, K. Ariga, T. Mori, Chemistry 14 (2008) 11529115–11529138.
[43] H. Gustafsson, C. Thörn, K. Holmberg, Colloids Surf. B Biointerfaces 87 (2011) 464–471.
[44] J. Lee, J. Kim, J. Kim, H. Jia, M.I. Kim, J.H. Kwak, S. Jin, A. Dohnalkova, H.G. Park, H.N. Chang, P. Wang, J.W. Grate, T. Hyeon, Small (2005) 744–753.
[45] S. Moreno-Pérez, A.H. Orrego, M. Romero-Fernández, L. Trobo-Maseda, S. Martins-DeOliveira, R. Munilla, G. Fernández-Lorente, J.M. Guisan, Methods Enzymol. 571 (2016) 55–72.
[46] D. Weber, A.J. Sederman, M.D. Mantle, J. Mitchell, L.F. Gladden, Phys. Chem. Chem. Phys. 12 (2010) 2619–2624.
[47] A. Salis, D. Meloni, S. Ligas, M.F. Casula, M. Monduzzi, V. Solinas, E. Dumitriu, Langmuir 21 (2005) 5511–5516.
[48] C. Mateo, J.M. Palomo, G. Fernandez-Lorente, J.M. Guisan, R. Fernandez-Lafuente, Enzyme Microb. Technol. 40 (2007) 1451–1463.
[49] R.C. Rodrigues, C. Ortiz, A. Berenguer-Murcia, R. Torres, R. Fernández-Lafuente, Chem. Soc. Rev. 42 (2013) 6290–6307.
[50] F. Secundo, Chem. Soc. Rev. 42 (2013) 6250–6261.
[51] M. Martínez-Martínez, C. Coscolín, G. Santiago, J. Chow, P. Stogios, R. Bargiela, C. Gertler, J. Navarro-Fernández, A. Bollinger, S. Thies, C. Méndez-García, A. Popovic, G. Brown, T.N. García Chernikova, A. García-Moyano, G.E.K. Bjerga, P. Pérez-García, T. Hai, M.V. Del Pozo, R. Stokke, I.H. Steen, H. Cui, X. Xu, B. Nocek, M. Alcaide, M. Distaso, V. Mesa, A.I. Peláez, J. Sánchez, P.C.F. Buchholz, J. Pleiss, A.F. Fernández-Guerra, F.O. Glöckner, O.V. Golyshina, M.M. Yakimov, A. Savchenko, K.-E. Jaeger, A.F. Yakunin, W.R. Streit, P.N. Golyshin, V. Guallar, M. Ferrer, ACS Chem. Biol. 13 (2018) 225–234.
[52] G. Santiago, M. Martínez-Martínez, S. Alonso, R. Bargiela, C. Coscolín, P.N. Golyshin, V. Guallar, M. Ferrer, Biochemistry 57 (2018) 2245–2255.
[53] L.E. Janes, C. Löwendahl, R.J. Kazlauskas, Chem. Eur. J. 4 (1998) 2317–2324.
[54] C. Coscolín, M. Martínez-Martínez, J. Chow, R. Bargiela, A. García-Moyano, G.E.K. Bjerga, A. Bollinger, R. Stokke, I.H. Steen, O.V. Golyshina, M.M. Yakimov, K.-E. Jaeger, A.F. Yakunin, W.R. Streit, P.N. Golyshin, M. Ferrer, Catalysts 8 (2018) 10.
[55] U.K. Laemmli, Nature 227 (1970) 680–685.
[56] M.M. Bradford, Anal. Biochem. 72 (1976) 248–254.
[57] P. Linton, V. Alfredsson, Chem. Mater. 20 (2008) 2878–2880.
[58] M. Thommes, K. Kaneko, A.V. Neimark, J.P. Olivier, F. Rodriguez-Reinoso, J. Rouquerol, K.S.W. Sing, Pure Appl. Chem. 87 (2015) 1051–1069.
[59] M.L. Ojeda, J.M. Esparza, A. Campero, S. Cordero, I. Kornhauser, F. Rojas, Phys. Chem. Chem. Phys. 5 (2003) 1859–1866.
[60] P.I. Ravikovitch, S.C.Ó. Domhnaill, A.V. Neimark, F. Schüth, K.K. Unger, Langmuir 11 (1995) 4765–4772.
[61] H. Yamamoto, A. Matsuyama, Y. Kobayashi, Biosci. Biotechnol. Biochem. 66 (2002) 481–483.
[62] D.A. Gaffney, S. O'Neill, M.C. O'Loughlin, U. Hanefeld, J.C. Cooney, E. Magner, Chem. Commun. 46 (2010) 1124–1246.